materials

MDPI

Article

Atomic Layer Deposition of $GdCoO_3$ and $Gd_{0.9}Ca_{0.1}CoO_3$

Marion Duparc, Henrik Hovde Sønsteby, Ola Nilsen, Anja Olafsen Sjåstad and Helmer Fjellvåg *

Centre for Materials Science and Nanotechnology, Department of Chemistry, University of Oslo, 0315 Oslo, Norway; m.j.l.duparc@smn.uio.no (M.D.); h.h.sonsteby@kjemi.uio.no (H.H.S.); ola.nilsen@kjemi.uio.no (O.N.); a.o.sjastad@kjemi.uio.no (A.O.S.)

* Correspondence: helmer.fjellvag@kjemi.uio.no

Received: 16 November 2019; Accepted: 16 December 2019; Published: 19 December 2019

Abstract: Thin films of the catalytically interesting ternary and quaternary perovskites $GdCoO_3$ and $Gd_{0.9}Ca_{0.1}CoO_3$ are fabricated by atomic layer deposition using metal β-diketonates and ozone as precursors. The resulting thin films are amorphous as deposited and become single-oriented crystalline on $LaAlO_3$(100) and $YAlO_3$(100/010) after post-annealing at 650 °C in air. The crystal orientations of the films are tunable by choice and the orientation of the substrate, mitigated through the interface via solid face epitaxy upon annealing. The films exhibit no sign of Co^{2+}. Additionally, high-aspect-ratio Si(100) substrates were used to document the suitability of the developed process for the preparation of coatings on more complex, high-surface-area structures. We believe that coatings of $GdCoO_3$ and $Gd_{1-x}Ca_xCoO_3$ may find applications within oxidation catalysis.

Keywords: gadolinium cobaltites; atomic layer deposition; β-diketonates; ozone; preferential crystal growth orientation; high-aspect-ratio substrate

1. Introduction

Rare-earth element perovskites with the formula ABO_3 (A = alkaline/ rare-earth element, B = 3d–5d transition metal) have received much attention in the field of heterogeneous catalysis [1–3]. The catalytic activity of these materials relates to the nature of the B-site element [2]. In addition, the partial substitution of the A-site alkaline/rare-earth element with a lower valency cation (typically Ca or Sr) may result in oxygen nonstoichiometry, which in turn induces specific effects on the catalytic performance [3]. Encouraging results for catalytic oxidation reactions have been obtained with $LaCoO_3$ and $La_{1-x}A'_xCoO_3$ (A' = Ca or Sr) [1,3]. However, the basicity of lanthanum makes such catalysts vulnerable to detrimental volume expansion due to lanthanum oxide hydration upon reaction with air and moisture [4,5]. Preliminary bench-scale catalyst performance tests of bulk $Gd_{1-x}Ca_xCoO_3$ for ammonia oxidation show comparable catalytic performance to the corresponding La-based system, but without the undesired degradation of the catalysts due to hydroxide formation upon temperature cycling in the processing atmosphere [6]. We currently focus on $GdCoO_3$-based catalysts of relevance for the ammonia slip reaction (i.e., the oxidation of minute quantities of NH_3 in a process stream into nitrogen and steam), owing to the lower basicity, and thus improved resistance towards hydration, of such Gd-containing compounds in realistic processing environments [7,8]. Notably, we also explore deposition routes for Ca-substituted variants, providing means for oxygen vacancies.

Recent literature underlines the pertinence of using atomic layer deposition (ALD) in the design and study of coatings for heterogeneous catalysis [9–11]. The sequential nature of the ALD technique inherently rules out any gas phase reactions, and the self-limiting nature of the processes leads to controllable and reproducible synthesis of morphologically and chemically uniform materials [12–14].

A major advantage of ALD compared to conventional thin-film synthesis routes like sputtering or CVD is the possibility of obtaining high-surface-area supported catalysts by depositing chemically uniform thin films of the active phase on a high-surface-area support [15,16]. This is enabled by the self-limiting mechanism that allows for deposition beyond the line-of-sight.

ALD processes have been developed and reported for a wide variety of oxides, including around 30 functional perovskites [17,18]. The development of ALD processes for ternary and quaternary oxides has recently gained attention due to their high potential in a range of applications, such as ferroelectrics, photovoltaics, and battery technology [18,19]. However, owing to the complexity of multi-cation deposition, the available ALD processes for quaternary oxides are still limited to a few systems [20]. To the best of our knowledge, no reports have been published on the preparation of ALD films of $GdCoO_3$ or the substituted variants thereof.

ALD of $LaCoO_3$ using β-diketonates and ozone was reported in 1997 by Seim et al. [21]. No reports were made of any structural or functional characterization of the product films. More recently, ALD of the quaternary $La_{1-x}Sr_xCoO_{3-\delta}$ system for the composition range $0.3 < x < 0.7$ was achieved by Ahvenniemi et al., using the same type of process [20]. One of the challenges of introducing cobalt in complex oxide ALD is catalytic decomposition of ozone and the metal-organic precursors by CoO_x species. This challenge can be overcome by tuning the precursor flux and precursor sequence, similar to recent reports on the deposition of lanthanum cuprate, for which CuO_x species exhibit the same detrimental catalytic precursor decomposition [22].

In this work we report for the first time the controlled thin-film growth and characterization of the ternary $GdCoO_3$ and quaternary $Gd_{1-x}Ca_xCoO_3$ rare-earth cobaltites using β-diketonates and ozone as precursors on flat and high-aspect ratio substrates. The current investigation is a step towards the growth and tailoring of highly selective complex thin films for heterogeneous catalysis.

2. Experimental

2.1. ALD and Precursors

All thin films were deposited in a F-120 Sat reactor (ASM Microchemistry, Helsinki, Finland) at a reactor temperature of 300 °C, unless otherwise stated. The temperature was chosen to comply with applicable temperatures for the binary oxide processes. Nitrogen was used as a purging gas, supplied from gas cylinders (99.999%, Praxair Norway, Oslo, Norway) and run through a Mykrolis purifier (Avantor Fluid Handling LLC, Devens, MA, USA) to remove oxygen and water impurities. The purging gas was maintained at a 300 cm^3 min^{-1} flow rate, giving an operating pressure of 2.6 mbar throughout the process.

$Co(thd)_2$ (99.9+%, Volatec, Porvoo, Finland), $Gd(thd)_3$ (99.9%, Strem Chemicals Inc., Kehl, Germany) and $Ca(thd)_2$ (99.9+%, Volatec) were used as cation sources, maintained in open boats in the reactor at 115 °C, 140 °C, and 198 °C, respectively (thd = 2,2,6,6-tetramethyl-3,5-heptanedionate). All precursors were re-sublimated before use to enhance purity. O_3 was used as the oxygen source, made from O_2 gas (99.6%, Praxair Norway) with an In USA (AC-2505) ozone generator producing 15 mass% O_3 in O_2. Pulse durations were set to 1.5 s for all metal precursors, whereas ozone was pulsed for 5 s subsequent to $Co(thd)_2$ and 3 s subsequent to $Gd(thd)_3$ and $Ca(thd)_2$ pulses. All purge durations were set to 2 s. The pulse and purge durations were chosen in agreement with previous reports of self-limiting growth using these precursors in similar reactor infrastructures.

2.2. Substrates and Annealing

Films were routinely deposited on 1 × 1 cm^2 Si(100) for characterization of thickness, whereas 3 × 3 cm^2 Si(100) substrates were used for compositional analysis with X-ray fluorescence (XRF) and for investigating any thickness gradients. Selected films were deposited on 1 × 1 cm^2 $LaAlO_3$ $(100)_{pseudocubic}$ (LAO, MTI Corp., Richmond, CA, USA), $YAlO_3$ (100) (MTI Corp.) and $YAlO_3$ (010) (YAP, MTI Corp.) for the facilitation of epitaxial growth. The investigation of conformality on

high-aspect-ratio substrates was carried out on silicon substrates with parallel grooves of 20 µm depth and 10 µm width (SINTEF IKT made by reactive ion etching with the Bosch process).

The selected films were annealed at 650 °C for 30 min in 1 atm air in an OTF-1200X rapid thermal processing (RTP) furnace (MTI Corp., Richmond, CA, USA) to facilitate crystallization prior to structural investigation.

2.3. Characterization

Film thickness was routinely studied using a J. A. Woollam alpha-SE spectroscopic ellipsometer (J.A. Woollam Co., Lincoln, NE, USA) in the wavelength range 390–900 nm. A Cauchy function was successfully used to model the collected data.

X-ray diffraction (XRD) measurements were used to investigate the out-of-plane crystalline orientation of the thin films on single crystal substrates. Symmetric θ-2θ-scans were carried out on a Bruker AXS D8 Discover diffractometer (Bruker AXS, Karlsruhe, Germany) equipped with a LynxEye strip detector (Bruker AXS) and a Ge (111) focusing monochromator, providing CuKα_1 radiation.

Chemical composition was analyzed using a Panalytical Axios Max Minerals XRF system (Malvern Panalytical, Malvern, UK) equipped with a 4 kW Rh tube. Omnian and Stratos options were employed for standardless measurements of thin film cation composition.

The chemical state of the cations, particularly cobalt, was investigated by X-ray photoelectron spectrometry (XPS) using a Thermo Scientific Theta Probe Angle-Resolved XPS system (ThermoFisher Scientific, Waltham, MA, USA). The instrument was run with a standard Al Kα source (hν = 1486.6 eV), and the analysis chamber pressure was maintained on the order of 10^{-8} mbar. Pass energy values of 200 eV and 50 eV were employed for survey scans and detailed scans, respectively. The data were corrected for any drift by setting the binding energy for adventitious carbon to 284.8 eV. Data treatment and fitting were performed within the Avantage software suite (ThermoFisher Scientific). The background was fitted to a Shirley-type pseudostep function.

Cross section SEM images of the deposited films were obtained using a Hitachi SU8230 SEM (Hitachi, Krefeld, Germany) with a cold cathode field emission electron gun. The total voltage was set to 2 kV and the films were imaged by means of secondary and back-scattered electrons.

3. Results and Discussion

3.1. Deposition of $GdCoO_3$

The development of ternary deposition processes typically requires insight into the individual growth behavior of the binary components. ALD of Co_3O_4, using $Co(thd)_2$ as a precursor and ozone as the oxidizing agent, was established by Klepper et al. in the 114–307 °C temperature range, with a growth per cycle (GPC) of ≈ 0.20 Å/cycle at 300 °C [23]. For a similar $Gd(thd)_3$-based deposition process, Niinistö et al. reported self-limiting growth for Gd_2O_3 films in the range from 250 to 300 °C, with a GPC of ≈ 0.30 Å/cycle at 300 °C [24]. Our attempts at deposition of the same binary processes gave reproducible GPCs of 0.16 Å/cycle and 0.37 Å/cycle for the formation of CoO_x and Gd_2O_3, respectively, with no observed thickness gradients.

Based on these results, a series of (Gd, Co)-oxide films were deposited at 300 °C. The $Gd(thd)_3$: $Co(thd)_2$ pulsed ratio was varied systematically to identify the conditions required to obtain the desired deposited stoichiometry of $GdCoO_3$. We employed a super cycle approach with a general super cycle, given as:

$$n \times \{m \times [Gd(thd)_3 + O_3] + l \times [Co(thd)_2 + O_3]\}, \quad (1)$$

where n, m, and l were varied to achieve the desired cation ratio.

Figure 1 shows the deposited cation ratio for Gd (cat.% Gd) of the obtained film and the GPC as a function of the pulsed cation ratio (cat.% Gd) at 300 °C. The relative amount of deposited Gd increases from 2 to 51 cat.% Gd in the explored pulsed cation range of 33–67 cat.% Gd. The concentration of Gd in the deposited film consistently increases with increasing amounts of pulsed $Gd(thd)_3$, except for the

plateau interval observed between 50 and 56 cat.% Gd pulsing ratio, where the Gd concentration in the product takes a constant value at around 32 cat.%. We note that the desired Gd:Co ratio of close to unity is obtained for 67 cat.% of pulsed Gd. The GPC of the deposited films at 300 °C increases smoothly with an increased fraction of Gd pulses, in accordance with the higher GPC of Gd_2O_3, see Figure 1. However, an excess of Gd pulses must be applied to achieve stoichiometric $GdCoO_3$. We do observe a small reduction in overall GPC (0.24 Å/cycle) as compared to a linear combination of the binary oxides [(0.37 + 0.16)/2 = 0.27 Å/cycle], possibly due to either inhibition of growth from $Gd(thd)_3$ on Co-O* surfaces or by increased growth from $Co(thd)_2$ on Gd-O* surfaces, or most likely a combination of both judging from the dependency of pulsed to deposited composition in Figure 1. This is an effect seen in several ALD processes, such as reported earlier by our group in the case of $LaAlO_3$ [25]. The GPCs obtained at 300 °C for (Gd, Co)-oxides are in good agreement with the results of Seim et al., who reported an average GPC of 0.35 Å/cycle for $LaCoO_3$ at 350 °C following a similar β-diketonate and ozone deposition process [21].

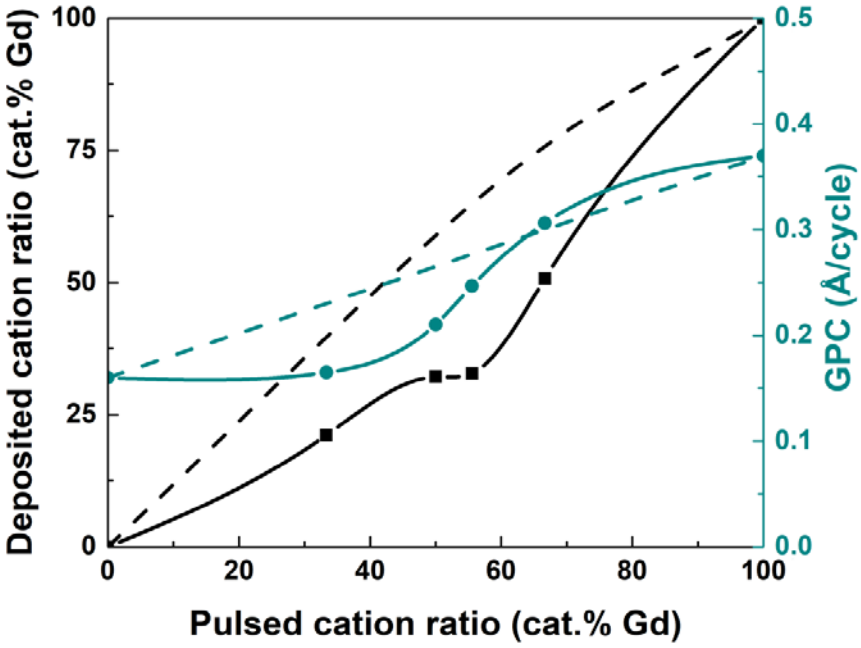

Figure 1. Deposited cation ratio (cat.% Gd, as measured by XRF) and GPC as a function of the pulsed cation ratio (cat.% Gd) for (Gd, Co)-oxide films deposited at 300 °C. The dotted lines refer to deposited cation ratio (cat.% Gd) and GPC as a function of the pulsed cation ratio (cat.% Gd) for Gd_2O_3 film.

3.2. Deposition of $Gd_{1-x}Ca_xCoO_3$

Based on the results obtained for the ternary (Gd, Co)-oxide system, the quaternary (Gd, Ca, Co)-oxide system was explored in an attempt to target products with the $Gd_{0.9}Ca_{0.1}CoO_3$ composition. ALD was carried out at 300 °C following an identical process as for ternary (Gd, Co)-oxide films, with the essential modification of substituting a number of $Gd(thd)_3$-pulses with $Ca(thd)_2$-pulses. The [$Gd(thd)_3$ + $Ca(thd)_2$]: $Co(thd)_2$ pulsed ratio was maintained at 2:1 in order to keep the deposited (Gd + Ca): Co atomic ratio close to unity. The Ca pulsed ratio, using $Ca(thd)_2$ as precursor, was varied from 3 to 7 cat.%. Figure 2a shows the deposited cation ratios and the GPC as a function of the Ca pulsed ratio (cat.%) for depositions at 300 °C. The Ca content in the films correlates fairly well with the relative amount of Ca pulses. In a few experiments deviating behavior was observed, which reflects the challenge of controlling the simultaneous growth of three different cation species [26]. However, quite a stable growth situation was obtained for the range around 4–5 cat.% Ca. The A-site (Gd + Ca): B-site (Co) stoichiometry was analyzed as function of the relative amount of Ca-pulses (Figure 2b). With the current pulsing strategy, the target (Gd + Ca): Co ratio close to unity is obtained for

films deposited at a Ca pulsed ratio between 3.5 and 5 cat.%. The targeted composition $Gd_{0.9}Ca_{0.1}CoO_3$ is obtained for a Ca pulsed ratio of 4.5 cat.%, for which an equiatomic ratio is maintained between the perovskite A- and B-sites.

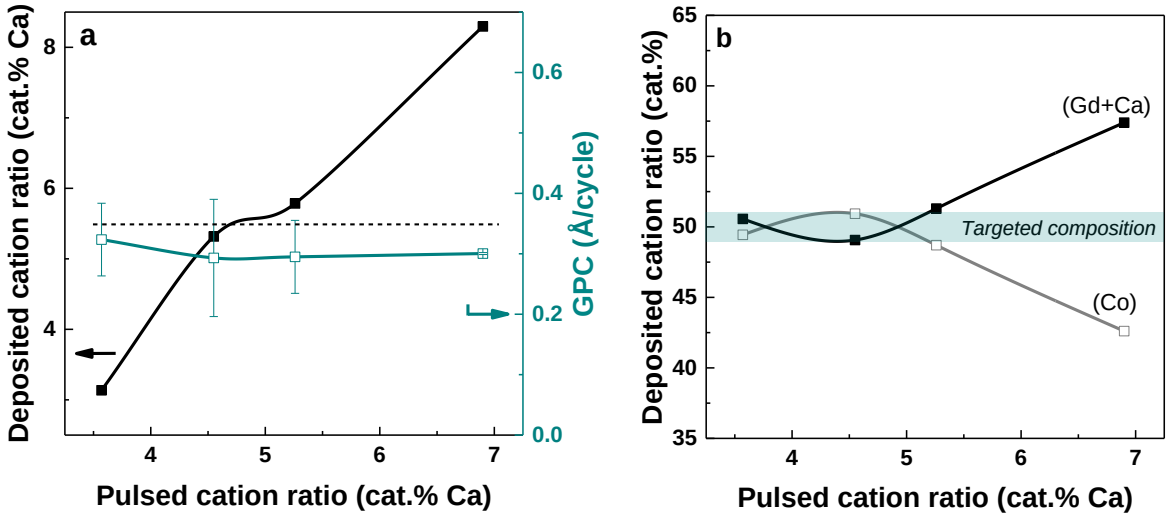

Figure 2. (**a**) Deposited cation ratio (cat.% Ca, as measured by XRF) and (**b**) GPC deposited cation ratio (cat. % (Gd + Ca) and Co, as measured by XRF) as a function of the pulsed cation ratio (cat.% Ca) for (Gd, Ca, Co) films deposited at 300 °C. The dotted line indicates the targeted Ca deposited concentration.

3.3. Characterization of $GdCoO_3$ and $Gd_{0.9}Ca_{0.1}CoO_3$ Thin Films

3.3.1. X-Ray Diffraction (XRD)

The as-prepared $GdCoO_3$ and $Gd_{0.9}Ca_{0.1}CoO_3$ films deposited at 300 °C are X-ray amorphous. Crystallization is achieved upon annealing at 650 °C for 30 min in air on LAO and YAP single crystals, resulting in preferential orientation depending on the substrate type and orientation. Figure 3a,b shows XRD patterns of post-annealed $GdCoO_3$ and $Gd_{0.9}Ca_{0.1}CoO_3$ films deposited on $LAO(100)_{pc}$. The diffractograms for the crystalline films on $LAO(100)_{pc}$ can be indexed as orthorhombic $GdCoO_3$ (*Pbnm*, SG# 62; Z = 4) with a preferred (010) growth orientation. The orthorhombically distorted $GdCoO_3$ perovskite relates to the ideal cubic perovskite structure (*Pm-3m*; Z = 1) as $a_o = \sqrt{2} \times a_c$, $mboxemphb_o = 2 \times b_c$, $c_o = \sqrt{2} \times c_c$ with dimensions a_o = 5.380 Å, b_o = 7.437 Å and c_o = 5.210 Å. The (rhombohedral) LAO substrate exhibits a pseudo cubic structure a_c = 3.79 Å (note $\sqrt{2} \times a_c$ = 5.36 Å). The growth of $GdCoO_3$-based perovskites onto LAO is favored in the (010) orientation as the *a*- and *c*-axis of the film match the diagonals of the cube faces of the substrate. In this configuration, $GdCoO_3$ will experience a lattice expansion of 2.5% in order to match the diagonal by diagonal area of the LAO substrate ($A_{LAO} = a_c^2$ = 28.73 Å^2 and $A_{GCO} = a_o \times c_o$ = 28.02 Å^2). The position of the (020) and (040) reflections indicate that $b_{GCO||LAO(100)}$ = 7.42 Å (strain−0.2%), which indicates a small compression compared to the theoretical orthorhombic structure. This is in good agreement with the expected expansion in *a*. We used Scherrer's formula on the well-defined $GdCoO_3$ (040) reflection (Supporting Figure S1) to estimate a crystallite size of 24.8 nm, which indicates that the crystallites traverse from the substrate to the film surface. A higher degree of crystallinity is observed for $GdCoO_3$, which exhibits sharper and more intense (020) and (040) reflections than $Gd_{0.9}Ca_{0.1}CoO_3$. This is in good agreement with Bretos et al., who reported a slower crystallization process for Ca-substituted perovskites [27].

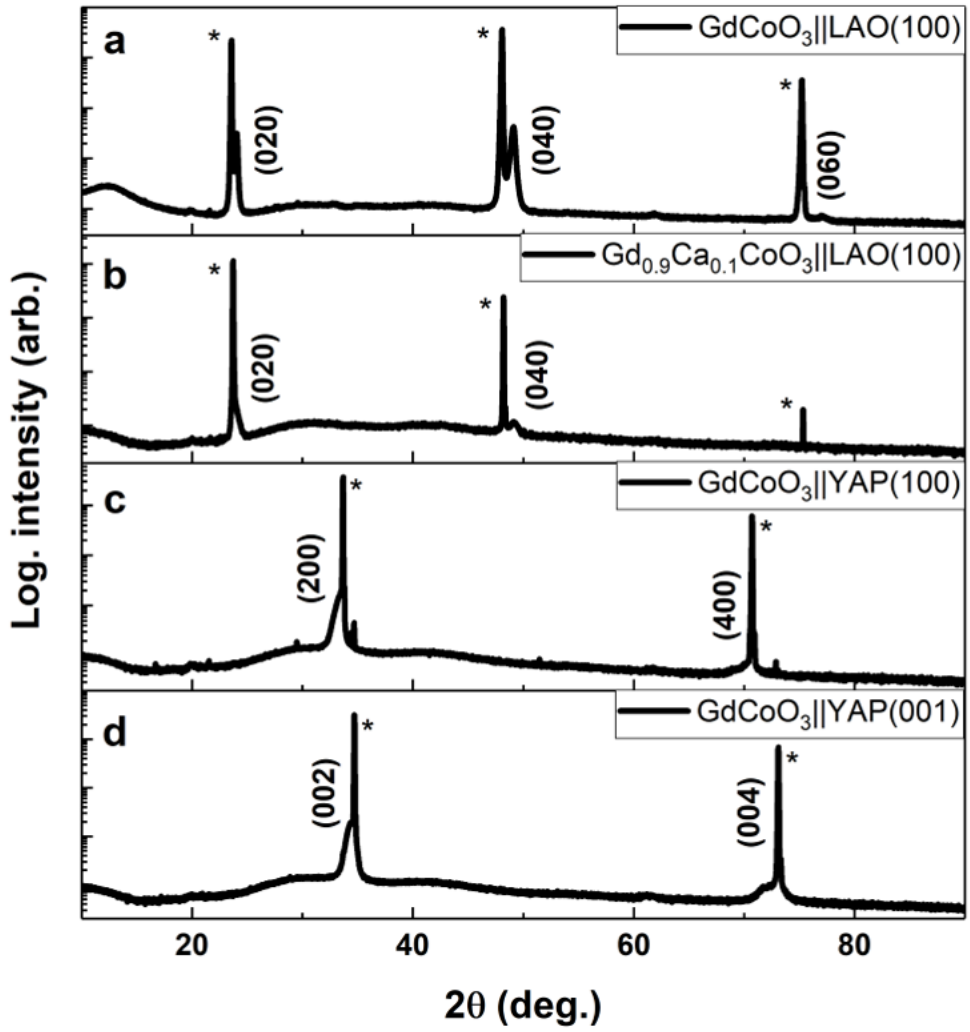

Figure 3. XRD patterns of (**a**) 30 nm $GdCoO_3$ and (**b**) 30 nm $Gd_{0.9}Ca_{0.1}CoO_3$ films grown on LAO(100), (**c**) 30 nm $GdCoO_3$ grown on YAP(100) and (**d**) 30 nm $GdCoO_3$ grown on YAP(001), post-annealed for 30 min at 650 °C. Bragg reflections originating from the substrate are marked with a star; film reflections are marked with their designated plane of reflection.

Figure 3c,d shows the measured XRD patterns from crystalline $GdCoO_3$ films deposited on YAP (100) and YAP (001), respectively, after post annealing at 650 °C in air for 30 min. Both YAP and $GdCoO_3$ are orthorhombic perovskites and exhibit quite similar unit cell dimensions; for YAP, a_{YAP} = 5.330 Å, b_{YAP} = 7.375 Å and c_{YAP} = 5.180 Å. $GdCoO_3$ deposited on YAP(001) grows with a preferred (001) orientation, whereas $GdCoO_3$ deposited on YAP(100) exhibits a preferential (100) growth orientation. Thus, the preferential (001) growth orientation of $GdCoO_3$ onto an oriented YAP(001) substrate is favored due to a minimized lattice compressive stress of 1.7% in this configuration ($V_{YAP(001)} = a_{YAP} \times b_{YAP}$ = 39.31 Å^2 and $V_{GCO} = a_o \times b_o$ = 39.97 Å^2). On the other hand, a (100) orientation of the substrate results in the growth of $GdCoO_3$ in a preferential (100) orientation with a lattice compression of 1.2% ($V_{YAP(100)} = b_{YAP} \times c_{YAP}$ = 38.20 Å^2 and $V_{GCO} = b_o \times c_o$ = 38.64 Å^2). The close lattice match means that the film reflections are observed as a broadening of the substrate peaks, making it difficult to analyze the diffraction in terms of crystallite size or strain. The $Gd_{0.9}Ca_{0.1}CoO_3$ thin films deposited on YAP substrates exhibited too poor a crystallinity, even after annealing, to be properly indexed (see Supplementary Figure S2).

By use of this appropriate selection of substrates, we have demonstrated the preferred crystallization along all three crystallographic axes. The effect of surface structure on catalytic

activity is well known, so the ability to select the growth orientation of crystalline films may be of high importance.

The physical properties of gadolinium cobaltites depend, inter alia, on the temperature and cation substitutions, type, and concentration, which in turn may have a profound effect on the catalytic performance. For instance, an expanded lattice triggered by the substrate may stabilize the high-spin Co(III) configuration at temperatures lower than 800 K, i.e., the transition temperature for bulk $GdCoO_3$ [28]. Such scenarios are interesting from an ALD perspective, since key physical and chemical performance properties may be tuned by the choice of appropriate lattice-matching substrates.

3.3.2. XPS

Detailed XPS spectra close to the Co 2p binding energies were collected to identify the chemical state of cobalt in the films (Figure 4). Previous reports of ALD-grown cobalt oxide using β-diketonates and ozone indicated a mixed $2^+/3^+$ valence. The presence of Co^{2+} could indicate detrimental inclusions of Co_3O_4 in the grown films. Co^{2+} can be identified by an intense shake-up satellite feature at around 786 eV, whereas the Co^{3+} satellite is shifted towards 790 eV. Currently, we only observed Co^{3+} satellite features, indicating that the films are dominated by $GdCoO_3$. Based on the data and the complexity of Co XPS, however, we cannot rule out that some Co^{2+} is present in the films. Survey spectra and detailed scans of O 1 s and C 1 s can be found in the Supplementary Materials (Figure S3).

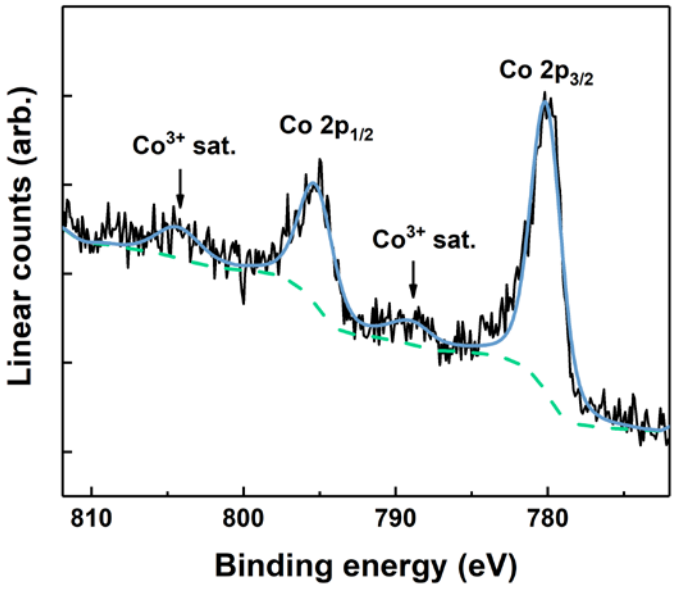

Figure 4. Co 2p XPS of 30 nm $GdCoO_3$ thin films on $LaAlO_3$ (100), with no observation of Co^{2+}. The black line is the recorded data, the green line is the background, and the light blue line is the total fit.

3.3.3. Deposition on a High-Aspect-Ratio Substrate

The ability to deposit catalytically active complex oxides on high aspect ratios is of high importance. This can, e.g., enable the coating of mesoporous γ-alumina, and thereby provide catalysts with a significantly enhanced surface area compared to nanoparticles (10–100 nm) obtained from wet chemical synthesis and/or ball milling. The conformality of the two gadolinium cobaltite-based films was investigated by applying the presented deposition process onto high-aspect-ratio substrates. Figure 5 shows cross section images of a $GdCoO_3$ film deposited on a high-aspect-ratio trench Si wafer. The film is conformally deposited on all surfaces of the substrate. As shown in Figure 5b, the bottom of the trench is characterized by the presence of agglomerates, possibly resulting from turbulence during growth and/or the preparation of cross section SEM samples.

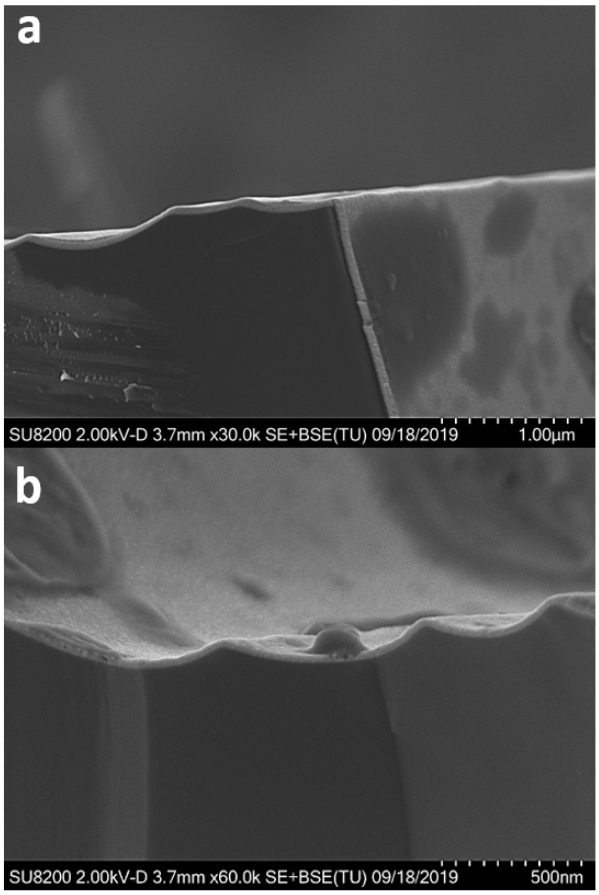

Figure 5. SEM cross-sectional images of $GdCoO_3$ deposited on a trench Si wafer: (**a**) top trench view; (**b**) bottom trench view.

4. Conclusions

We have developed an ALD process for crystalline and homogeneous Gd-Ca-Co-O thin films on three different substrates, which provides a route towards coatings with potential application within catalysis. The good crystallinity of the obtained films gives insight into the crystal structure of the product and orientation of crystallization, which is essential since catalytic performance depends on key parameters connected with the structure, chemistry, and electronic states of exposed surfaces. These features are shown to be tuned by appropriate choices of ALD precursors, substrates, and deposition/annealing conditions. The proof of concept of depositing conformal Gd-Ca-Co-O films on high-aspect-ratio substrates is important, since practical applications in catalysis would require high surface areas.

The gadolinium cobaltite-based catalysts represent a particularly interesting system, not only with respect to catalysis, but also to physical properties. For instance, an expanded lattice triggered by the substrate may possibly stabilize a high-spin Co(III) state. Such scenarios suggest that ALD can be used to tune resulting properties by means of appropriate lattice-matching substrates.

Supplementary Materials: The following are available online at http://www.mdpi.com/1996-1944/13/1/24/s1: Figure S1: XRD patterns of 30 nm $Gd_{0.9}Ca_{0.1}CoO_3$ films grown on (a) YAP(100) and (b) YAP(001), post-annealed for 30 minutes at 650 °C. Figure S2: XRD pattern of the $GdCoO_3$ (040) reflection of as deposited (black) and annealed (green) 30 nm films grown on LAO $(100)_{pc}$, used for Scherrer analysis of crystallite size. Figure S3: (a) XPS of C 1s, (b) XPS of O 1s and (c) Survey spectra showing identification of Gd, Co, O and carbon species.

Author Contributions: Investigation, M.D. and H.H.S.; formal analysis, M.D. and H.H.S.; methodology, H.H.S. and O.N.; project administration, O.N., A.O.S. and H.F.; writing—original draft preparation, M.D.; writing—review and editing, M.D., H.H.S., O.N., A.O.S. and H.F.; supervision, A.O.S. and H.F. All authors have read and agreed to the published version of the manuscript.

Funding: This project received financial support from the Research Council of Norway via the ASCAT project (contract no. 247753).

Acknowledgments: The authors acknowledge the Department of Geology at the University of Oslo for access to XRF instrumentation. Henrik H. Sønsteby acknowledges the Research Council of Norway for funding via the RIDSEM project (contract no. 272253). In addition, they thank Jon Einar Bratvold for his assistance with the ALD reactor, Kristian Weibye for recording XPS spectra, and Martin Jensen for recording SEM images.

Conflicts of Interest: The authors declare no conflict of interest.

References

1. Royer, S.; Duprez, D.; Can, F.; Courtois, X.; Batiot-Dupeyrat, C.; Laassiri, S.; Alamdari, H. Perovskites as Substitutes of Noble Metals for Heterogeneous Catalysis: Dream or Reality. *Chem. Rev.* **2014**, *114*, 10292–10368. [CrossRef] [PubMed]
2. Pena, M.A.; Fierro, J.L.G. Chemical Structures and Performance of Perovskite Oxides. *Chem. Rev.* **2011**, *101*, 1981–2018. [CrossRef] [PubMed]
3. Kim, C.H.; Qi, G.; Dahlberg, K.; Li, W. Strontium-doped perovskites rival platinum catalysts for treating NOx in simulated diesel exhaust. *Science* **2010**, *327*, 1624–1627. [CrossRef] [PubMed]
4. Fleming, P.; Farrell, R.A.; Holmes, J.D.; Morris, M.A. The Rapid Formation of $La(OH)_3$ from La_2O_3 Powders on Exposureto Water Vapor. *J. Am. Ceram. Soc.* **2010**, *93*, 1187–1194. [CrossRef]
5. Waller, D.; Grønvold, M.S.; Sahli, N. *Ammonia Oxidation Catalyst for the Production of Nitric Acid Based on Yttrium-Gadolinium Ortho Cobaltates*; World Intellectual Property Organization: New York, NY, USA, 2017.
6. Duparc, M.; et al. 2019; Unpublished manuscript.
7. Nagao, M.; Hamano, H.; Hirata, K. Hydration Process of Rare-Earth Sesquioxides Having Different Crystal Structures. *Langmuir* **2003**, *19*, 9201–9209. [CrossRef]
8. Krishnamurthy, N.; Gupta, C.K. *Extractive Metallurgy of Rare Earths*; CRC Press: Boca Raton, FL, USA, 2004.
9. Marichy, C.; Bechalany, M.; Pinna, N. Atomic Layer Deposition of Nanostructured Materials for Energy and Environmental Applications. *Adv. Mater.* **2012**, *24*, 1017–1032. [CrossRef]
10. O'Neill, B. Catalyst Design with Atomic Layer Deposition. *ACS Catal.* **2015**, *5*, 1804–1825. [CrossRef]
11. Camacho-Bunquin, J.; Shou, H.; Aich, P.; Beaulieu, D.R.; Klotzsch, H.; Bachman, S.; Marshall, C.L.; Hock, A.; Stair, P. Catalyst synthesis and evaluation using an integrated atomic layer deposition synthesis–catalysis testing tool. *Rev. Sci. Instrum.* **2015**, *86*, 84–103. [CrossRef]
12. Suntola, T. Atomic layer epitaxy. *Mater. Sci. Rep.* **1989**, *4*, 261–312. [CrossRef]
13. Leskelä, M.; Ritala, M. Atomic layer deposition (ALD): From precursors to thin film structures. *Thin Solid Films* **2002**, *409*, 138–146. [CrossRef]
14. George, S.M. Atomic layer deposition: An overview. *Chem. Rev.* **2009**, *110*, 111–131. [CrossRef] [PubMed]
15. Onn, T.M.; Dai, S.; Chen, J.; Pan, X.; Graham, G.W.; Gorte, R.J. High-Surface Area Ceria-Zirconia Films Prepared by Atomic Layer Deposition. *Catal. Lett.* **2017**, *147*, 1464–1470. [CrossRef]
16. Onn, T.M.; Monai, M.; Dai, S.; Arroyo-Ramirez, L.; Zhang, S.; Pan, X.; Graham, G.W.; Fornasiero, P.; Gorte, R.J. High-surface-area, iron-oxide films prepared by atomic layer deposition on γ-Al_2O_3. *Appl. Catal. A Gen.* **2017**, *534*, 70–77. [CrossRef]
17. Miikkulainen, V.; Leskelä, M.; Ritala, M.; Puurunen, R.L. Crystallinity of inorganic films grown by atomic layer deposition: Overview and general trends. *J. Appl. Phys.* **2013**, *113*, 2. [CrossRef]
18. Sønsteby, H.H.; Fjellvåg, H.; Nilsen, O. Functional Perovskites by Atomic Layer Deposition—An Overview. *Adv. Mater. Interfaces* **2017**, *4*, 1600903. [CrossRef]
19. Johnson, R.W.; Hultqvist, A.; Bent, S.F. A brief review of atomic layer deposition: From fundamentals to applications. *Mater. Today* **2014**, *17*, 236–246. [CrossRef]
20. Ahvenniemi, E.; Matvejeff, M.; Karppinen, M. Atomic layer deposition of quaternary oxide $(La,Sr)CoO_{3-\delta}$ thin films. *Dalton Trans.* **2015**, *44*, 8001–8006. [CrossRef]
21. Seim, H.; Nieminen, M.; Niinistö, L.; Fjellvåg, H.; Johansson, L.S. Growth of $LaCoO_3$ thin films from β-diketonate precursors. *Appl. Surf. Sci.* **1997**, *112*, 243–250. [CrossRef]
22. Sønsteby, H.H.; Bratvold, J.E.; Weibye, K.; Fjellvåg, H.; Nilsen, O. Phase Control in Thin Films of Layered Cuprates. *Chem. Mater.* **2018**, *30*, 1095–1101. [CrossRef]

23. Klepper, K.B.; Nilsen, O.; Fjellvåg, H. Growth of thin films of Co_3O_4 by atomic layer deposition. *Thin Solid Fims* **2007**, *515*, 7772–7781. [CrossRef]
24. Niinistö, J.; Petrova, N.; Putkonen, M.; Niinistö, L.; Arstila, K.; Sajavaara, T. Gadolinium oxide thin films by atomic layer deposition. *J. Cryst. Growth* **2005**, *285*, 191–200. [CrossRef]
25. Sønsteby, H.H.; Østreng, E.; Fjellvåg, H.; Nilsen, O. Deposition and x-ray characterization of epitaxial thin films of $LaAlO_3$. *Thin Solid Films* **2014**, *550*, 90–94. [CrossRef]
26. Leskelä, M.; Ritala, M.; Nilsen, O. Novel materials by atomic layer deposition and molecular layer deposition. *MRS Bull.* **2011**, *36*, 877–884. [CrossRef]
27. Bretos, I.; Ricote, J.; Jiménez, R.; Mendiola, J.; Jiménez Riobóo, R.J.; Calzada, M.L. Crystallisation of $Pb_{1-x}Ca_xTiO_3$ ferroelectric thin films as a function of the Ca^{2+} content. *J. Eur. Ceram. Soc.* **2005**, *25*, 2325–2329. [CrossRef]
28. Orlov, Y.S.; Solovyov, L.A.; Dudnikov, V.A.; Fedorov, A.S.; Kuzubov, A.A.; Kazak, N.V.; Voronov, V.N.; Vereshchagin, S.N.; Shishkina, N.N.; Perov, N.S.; et al. Structural properties and high-temperature spin and electronic transitions in $GdCoO_3$: Experiment and theory. *Phys. Rev. B* **2013**, *81*, 235105. [CrossRef]

© 2019 by the authors. Licensee MDPI, Basel, Switzerland. This article is an open access article distributed under the terms and conditions of the Creative Commons Attribution (CC BY) license (http://creativecommons.org/licenses/by/4.0/).